Distinguishing between folding and tearing mechanisms in strange attractors

Greg Byrne,[1] Robert Gilmore,[1] and Christophe Letellier[2]
[1]*Physics Department, Drexel University, Philadelphia, Pennsylvania 19104, USA*
[2]*CORIA UMR 6614–Université de Rouen, Boîte Postale 12, Avenue de l'Université, Saint-Etienne du Rouvray Cedex, France*
(Received 16 April 2004; published 19 November 2004)

We establish conditions for distinguishing between two topologically identical strange attractors that are enclosed by identical bounding tori, one of which is generated by a flow restricted to that torus, the other of which is generated by a flow in a different bounding torus and either imaged or lifted into the first bounding torus.

DOI: 10.1103/PhysRevE.70.056214 PACS number(s): 05.45.−a

I. INTRODUCTION

The important properties of dynamical systems, and the strange attractors they may generate, are invariant under a smooth change of coordinates [1–3]. These include the number and type of fixed points and their stability; geometric properties, such as fractal dimension; dynamical properties, such as Lyapunov exponents; and topological properties, such as topological entropy and the stretching and squeezing mechanisms that generate strange attractors. These mechanisms are understood in R^3, where they are described by branched manifolds. Branched manifolds summarize the stretching and squeezing mechanisms that act repetitively to build up strange attractors and to organize all their unstable periodic orbits in a unique way [4,5]. For this reason, they have been used to characterize low-dimensional strange attractors, namely those with Lyapunov dimension $d_L<3$ [6].

Local diffeomorphisms identify n points ($n>1$) in one phase space [R^3 (cover)] with a single point in another phase space [R^3 (image)] of the same dimension. Under a local diffeomorphism, some of the properties of a strange attractor are preserved and others are not. The number of fixed points typically changes, while the stability of their images (or covers) does not; geometric properties, fractal properties, dynamical properties, and topological entropy are preserved but global topological properties are not [7,8].

Local diffeomorphisms are often related to symmetries. For example, if a dynamical system in R^3 is equivariant (unchanged) under rotations by π radians about the z axis [$R_z(\pi)$], the $2\rightarrow 1$ local diffeomorphism

$$u = x^2 - y^2,$$

$$v = 2xy,$$

$$w = z, \tag{1}$$

identifies pairs of rotation-related points off the z axis in the covering phase space $R^3(x,y,z)$ with a single point in the image phase space $R^3(u,v,w)$ [7,8]. This transformation maps a strange attractor with $R_z(\pi)$ symmetry to an image strange attractor without symmetry. The two attractors are locally identical. By the inverse process, an image attractor without symmetry [with variables (u,v,w)], can be "lifted" to a covering attractor with symmetry [and coordinates (x,y,z)].

In this work, we investigate two related questions. (i) Suppose a covering attractor (Lorenz) is mapped to an image, so that it looks topologically like a Rössler attractor. How is it possible to distinguish this image from a Rössler attractor? (ii) Suppose a Rössler attractor is lifted to a covering attractor. How is it possible to distinguish this lift from an attractor generated by an equivariant set of equations?

We resolve both questions by investigating the return maps of the attractors. These carry very clear signatures of the stretching and squeezing mechanisms that generate chaos. These are the stretching and folding mechanism that occurs in Rössler-like attractors, and the stretching and tearing (and sometimes folding) mechanism, which occurs when a symmetry is present.

Our results depend on two powerful tools that are used to characterize strange attractors that exist in three-dimensional spaces. These tools are branched manifolds and bounding tori. In Sec. II, we review these structures and introduce their properties that are relevant to the content of this work. In Sec. III, we study return maps for strange attractors generated by flows in a bounding torus of genus 1 [9,10]. For highly dissipative dynamical systems, these look like smooth curves with differentiable local extrema. In Sec. IV, we study return maps for strange attractors generated by flows with $R_z(\pi)$ symmetry. These flows exist in a torus of genus 3. The Poincaré section consists of two generally disjoint components, and the return map describes how initial conditions on each component are mapped to these components [9,10]. In Sec. V, we compare image dynamics with dynamics in a genus-1 flow. The two differ in that for one the extrema in the return map are differentiable, for the other they are not. In Sec. VI, we compare covering dynamics with the dynamics of a typical strange attractor that can be generated in a genus-3 bounding torus. Return maps for both exhibit discontinuities. They differ in that in one case the one-sided derivatives at the discontinuity are equal, in the other case they are not. We summarize our results in Sec. VII.

II. BACKGROUND

The results presented in this work depend on two structures that have been used to describe strange attractors that can be generated by three-dimensional dynamical systems. These are branched manifolds and bounding tori. We summarize the properties of these two-dimensional objects that are most important for the purposes of the present work.

A. Branched manifolds

Birman and Williams [4,5] assume that a flow $\dot{x}=f(x)$, $x \in R^3$, generates a strange attractor. They identify two points, x and y, in phase space if they have the same asymptotic future under f,

$$x \sim y \text{ if } |x(t)-y(t)| \overset{t\to\infty}{\to} 0,$$

where $x(0)=x$ and $y(0)=y$. This has the effect of projecting the strange attractor along the stable direction onto a two-dimensional structure called a branched manifold. This fails to be a manifold because of singularities intrinsic to the dynamics: splitting points and branch lines [6]. The flow that generates the strange attractor is projected to a semiflow $\overline{f}$ on the branched manifold. The Birman-Williams theorem states that the topological organization of the unstable periodic orbits in the strange attractor (generated by f) remains unchanged under the projection to the branched manifold (generated by $\overline{f}$). This means, roughly speaking, that the stretching and squeezing mechanisms that act repetitively in phase space to build up the strange attractor (and simultaneously organize all the unstable periodic orbits in it) are preserved under the Birman-Williams projection. As a result, branched manifolds can be used to identify strange attractors [6]. Since branched manifolds are discretely classifiable (by integers), strange attractors are also discretely classifiable.

B. Bounding tori

Tsankov and Gilmore [9,10] have shown that branched manifolds can be fattened up by surrounding each point in them by a small ball of radius ε. The semiflow $\overline{f}$ on the branched manifold can simultaneously be extended to a flow $\tilde{f}$ on this three-dimensional manifold. This three-dimensional manifold is a handlebody of genus g (a bounded three-dimensional manifold with g nonintersecting holes drilled through it) in which the branched manifold is embedded. Its boundary is a torus of genus g. The flow $\tilde{f}$ is into this surface, and once inside this surface the flow is attracted exponentially to the branched manifold. The handlebody is an inertial manifold for the branched manifold and its boundary is a trapping surface: once the flow enters, it never gets out. Tsankov and Gilmore have also shown that it is possible to provide a canonical form for the flow on the genus-g surface. The canonical form is a projection of this two-dimensional surface onto a plane. In this projection, the genus-g torus appears as a disk with g interior holes. The flow is nonsingular on the (outer) disk boundary as well as on m of the interior holes, and is in the same direction (e.g., clockwise) on all $m+1$ boundaries. On the remaining $n=g-m$ interior holes there is an even number of singularities: 4, 6, …. The total number of singularities on the surface of this genus-g bounding torus is $2(g-1)$. Bounding tori have either $g=1$ or $g \geqslant 3$.

C. Branch lines in Poincaré sections

Branched manifolds organize periodic orbits that can exist in them in a very specific way [4–6]. So also do bounding tori organize branched manifolds that can exist in them in a very specific way [9,10]. A bounding torus with $g=1$ has a Poincaré surface consisting of one disk that is transverse to the flow $\tilde{f}$. The Poincaré surface for a bounding torus of genus $g \geqslant 3$ consists of $g-1$ disjoint disks. The locations of these disks are severely constrained by the singularities of the flow $\tilde{f}$ on the boundary. Each branch line for a branched manifold contained in a genus-g torus can be moved to one of the components of the global Poincaré surface of section. In the canonical projection, each component of the Poincaré surface appears as an interval connecting the boundary of one of the m interior holes without singularities to the exterior disk boundary. We use this fact to provide a natural orientation for the branch line ($g=1$) or $g-1$ branch lines ($g>1$) for branched manifolds contained in a genus-g torus. Each branch line can be parametrized by a real number x, $0 \leqslant x \leqslant 1$, with $x=0$ corresponding to the interior boundary and $x=1$ corresponding to the exterior boundary. We use this order to provide a natural structure for the return map when the Poincaré surface has more than one disconnected component (see Sec. II D). Suitable modifications can be made when the intersection of the branched manifold with a component of the Poincaré section does not have the topology of an interval but that of a circle S^1, as occurs for the driven van der Pol oscillator [6]. However, this does not occur for any of the dynamical systems treated below, so these details will not be treated here.

D. Structure of return maps

A strange attractor contained in a genus-1 bounding torus has a single disk as a Poincaré surface of section and its branched manifold has a single branch line that can be moved so that it lies in this disk. The return map of the branch line onto itself is a typical one-dimensional map, i.e., a logistic map for a horseshoe mechanism (cf., Fig. 1). To create this return map, the branch line can be parametrized from zero ("inside") to one ("outside"). The x coordinate ($0 \leqslant x \leqslant 1$) on this branch line is mapped to the y coordinate ($0 \leqslant y \leqslant 1$) according to its image, under the semiflow, when it returns to the branch line.

For more complicated attractors ($g \geqslant 3$), the return map is slightly more complicated. The global Poincaré surface of section consists of $g-1$ disjoint disks. The branched manifold for the attractor has $g-1$ branch lines, each of which can be moved into one of the disks. The $g-1$ branch lines can be numbered in a canonical way [10], from 1 to $g-1$, according to the order they are encountered following the outer disk boundary in the direction of the flow from any initial posi-

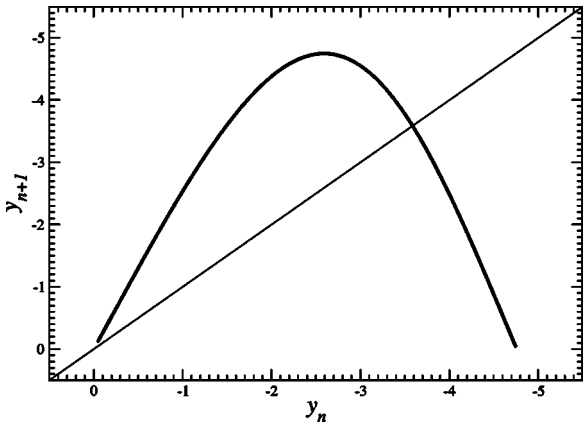

FIG. 1. First return map for the Rössler attractor. Parameter values: $(a,b,c)=(0.432,2.0,4.0)$.

tion. These $g-1$ disjoint intervals can be laid out along a horizontal axis. A coordinate x_k, $0 \leqslant x_k \leqslant 1$, identifies an initial condition at x_k on the kth branch line. A space could be placed between each of the $g-1$ horizontal intervals to emphasize that they are disjoint. We did not do that here in the interest of economizing space. Initial conditions along branch line k flow to two other branch lines that are identified by the transition matrix [9,10] for the bounding torus. As in the genus-1 case, the image is indicated along the vertical axis. Images can occur on $g-1$ branch lines. These are arranged as $g-1$ vertical intervals. A space between each can be included to emphasize that they are disjoint (we did not). Under the semiflow, the source point x_k first encounters branch line j at the unique point $y_j=f(x_k)$ after one (topological) period. The return map has the structure of a set of curves over the $g-1$ disjoint intervals. The curve over any one horizontal interval extends over two vertical intervals. Thus, points y_j may have zero, one, two, or more preimages, and the return map $f(x)$ is not one to one. With the conventions adopted ($x_j=0$ inside of branch line j, $x_j=1$ outside of the same branch line), construction of return maps $f(x)$ for branched manifolds contained in genus-g bounding tori is canonical. Such maps are shown in Figs. 2(c), 3(c), 5(a), 10(b), and 11(b).

III. RÖSSLER-LIKE DYNAMICS

We begin our study by constructing a return map for the Rössler attractor [11]. This is done in the usual way. The Rössler equations

$$\dot{x} = -y - z,$$

$$\dot{y} = x + ay,$$

$$\dot{z} = b + z(x - c), \tag{2}$$

are integrated for control parameter values $(a,b,c)=(0.432,2.0,4.0)$ to generate a strange attractor. Intersections y_i with the y-z plane through x_c (the x coordinate of the

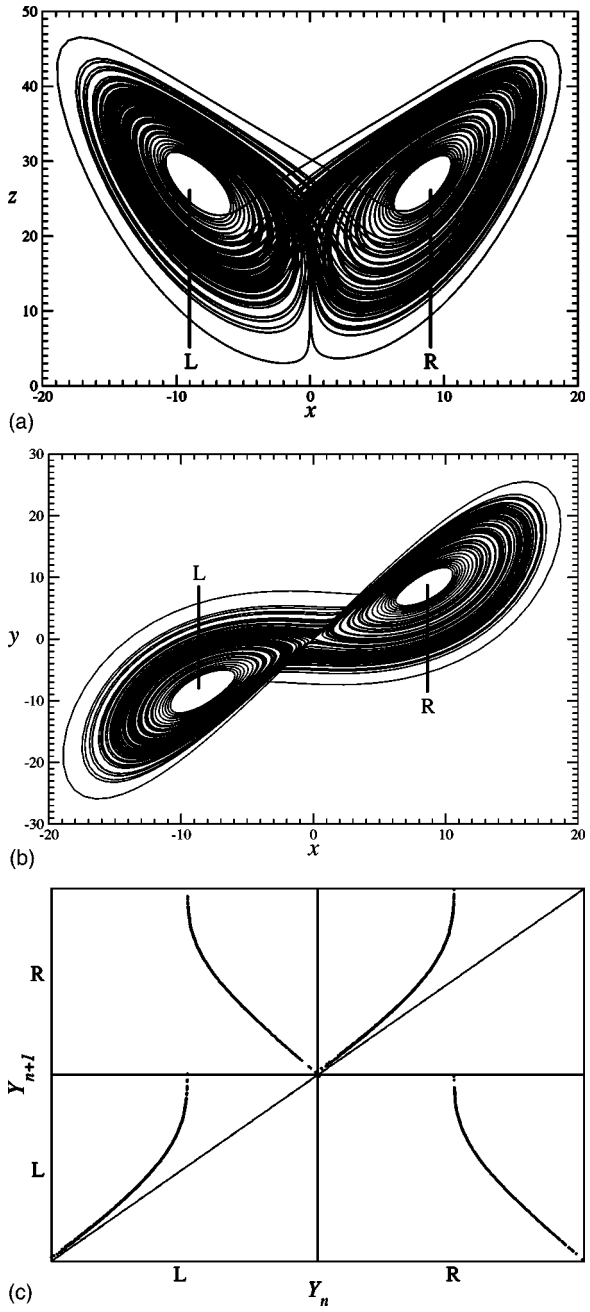

FIG. 2. Projection of the Lorenz attractor onto (a) the x-z plane and (b) the x-y plane. The two components of the global Poincaré section are shown. (c) Return map on the two components of the Poincaré section shows the branched manifold has four branchs. Tearing occurs. Parameter values: $(R,\sigma,b)=(28.0,10.0,8/3)$.

unstable focus near the origin) with $\dot{x}>0$ are recorded and used to create a first return map y_{i+1} versus y_i. This return map is shown in Fig. 1. The return map looks like a smooth, differentiable curve [6]. In fact, it has such an appearance because the Rössler attractor is highly dissipative. More generally, such a return plot would exhibit some fuzziness since the attractor is fractal. If the strange attractor is first projected onto a branched manifold and the intersection of this branched manifold with the Poincaré section were used to

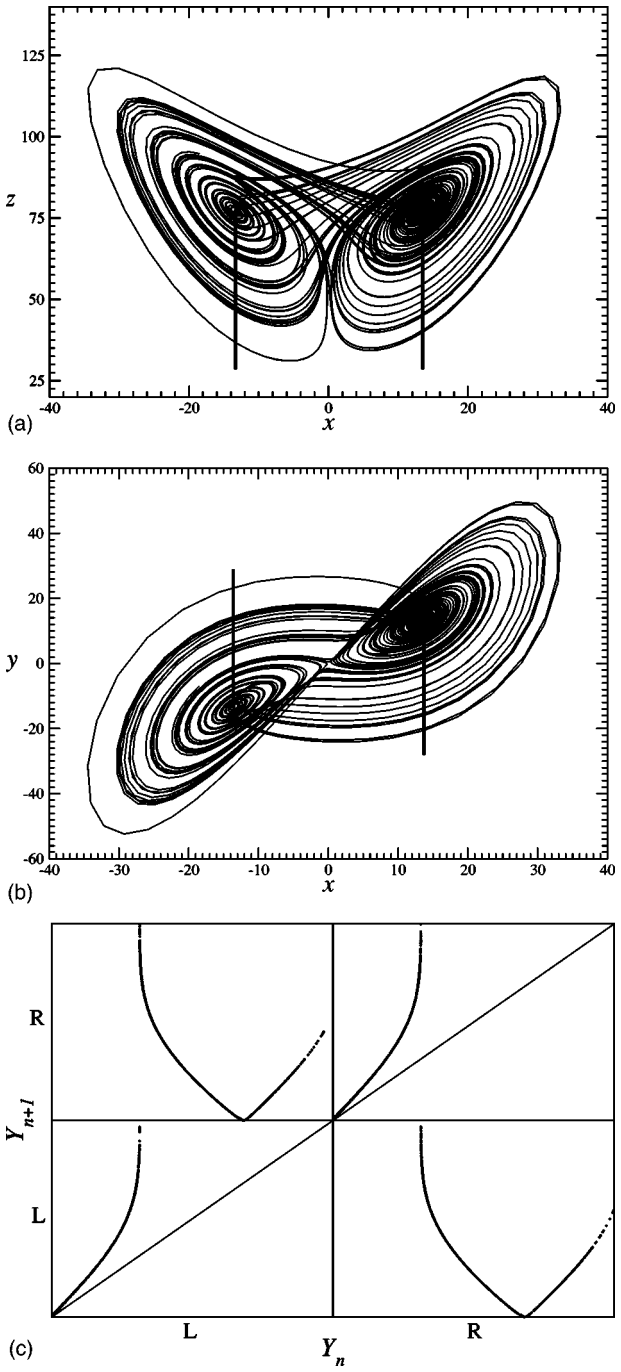

FIG. 3. Projection of the Lorenz attractor onto (a) the *x*-*z* plane and (b) the *x*-*y* plane. The two components of the global Poincaré section are shown. (c) Return map on the two components of the Poincaré section shows the branched manifold has six branches. Tearing and folding occur. Parameter values: $(R,\sigma,b)=(65.584,13.0,2.4167)$.

create a first return map, the result would rigorously be a smooth, differentiable curve. Here and below we use the return map for an attractor in place of a return map for the branched manifold since there is almost no observable difference between the two in the cases that we study.

The return map shown in Fig. 1 has a quadratic maximum. This occurs because as the flow spirals outward from the unstable focus near the origin, it must decelerate before being reinjected towards the unstable focus. In fact, this is a common property of all strange attractors contained in a bounding torus of genus 1 that are generated by smooth flows [9,10]. Each monotonic component of the return map can be identified with a branch of the characterizing branched manifold, and all monotonic segments are separated by a local maximum or minimum that is smooth, differentiable, and generically quadratic. Deceleration is responsible for horizontal tangents at extrema.

The mechanism responsible for creating chaos in the Rössler dynamical system and all similar dynamical systems (smooth forcing terms, strange attractor contained in a genus-1 torus) is stretching and folding. Differentiability of the return map at its critical points is the fingerprint characterizing folding.

IV. LORENZ-LIKE DYNAMICS

The Lorenz equations [12]

$$\dot{x} = -\sigma x + \sigma y,$$

$$\dot{y} = Rx - y - xz,$$

$$\dot{z} = -bz + xy, \tag{3}$$

were integrated for several different parameter values. Figures 2(a) and 2(b) show projections of the Lorenz attractor generated with parameter values $(R,\sigma,b)=(28.0,10.0,8/3)$ onto the *x*-*z* and the *x*-*y* planes. This attractor can be contained in a bounding torus of genus 3 [9,10]. The three (=genus) holes surround the two foci and the saddle at the origin. The global Poincaré section consists of two disconnected components. Both are shown in these figures. Figure 2(c) shows a return mapping of the Poincaré section to itself. The orientation of the two branch lines has been chosen in the natural way described in Sec. II: from inside (left) to outside (right). This return map shows that some of the initial conditions along the component of the Poincaré section near the focus on the left (L) return to the neighborhood of L (panel L-L), while initial conditions further away from this fixed point flow from L to R (panel L-R). Similar remarks hold, by symmetry, for flows originating on the component of the Poincaré section near the right-hand focus R. The discontinuity in the flow from L (and R) is the fingerprint for the stretching and tearing mechanism. In this case, the flow from L accelerates away from L, and as it nears the origin, it is split into a part that returns to L and a part that flows to a different component of the Poincaré section. The origin serves as a splitting singularity. The branched manifold for this attractor has four branches, one each describing the flows from $L\rightarrow L$, $L\rightarrow R$, $R\rightarrow L$, $R\rightarrow R$. Acceleration is responsible for nonhorizontal tangents at extrema.

Figure 3 is similar to Fig. 2, but for the Lorenz attractor generated for control parameter values $(R,\sigma,b)=(65.584,13.0,2.4167)$. The return map on the two compo-

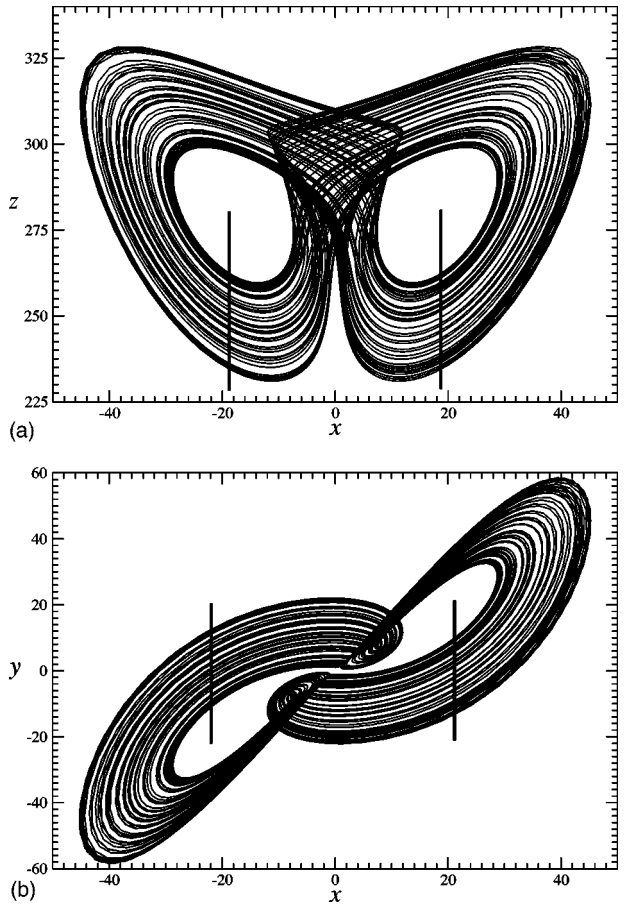

FIG. 4. Projection of the Lorenz attractor onto (a) the x-z plane and (b) the x-y plane. Parameter values: $(R,\sigma,b)=(278.56,30.0,1.0)$.

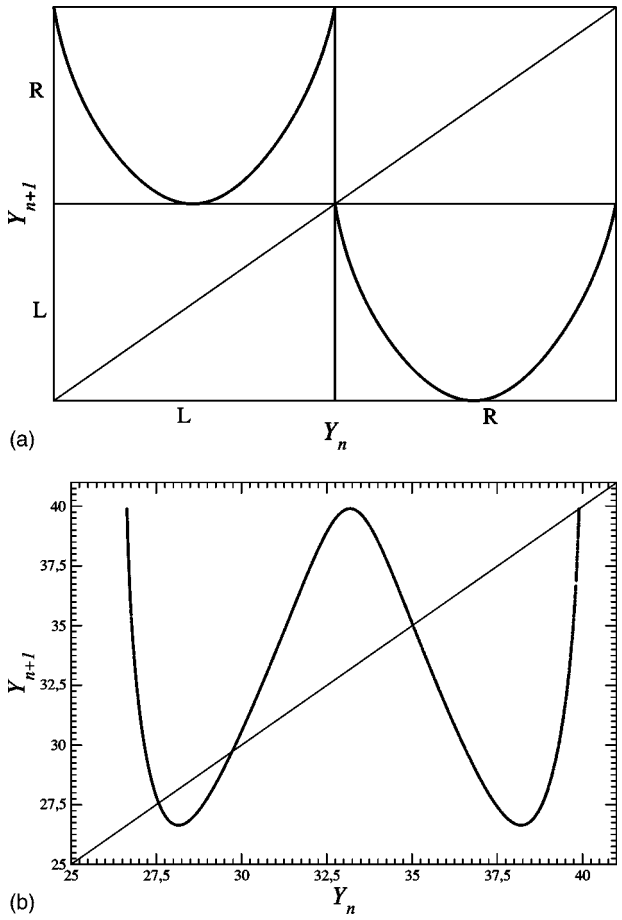

FIG. 5. First return maps for the Lorenz attractor shown in Fig. 4(a). The map onto the two components L and R shows that one component suffices. (b) The return map on a single component shows that stretching and folding is the operative mechanism. Both maps show the flow has four branches.

nents of the Poincaré section is shown in Fig. 3(c). In this case there is a discontinuity. It appears as the jump from L to R and the jump from R to L. Folding also occurs—it appears in the off-diagonal panels L-R and R-L in the return map. This return map shows clearly that the strange attractor, for these parameter values, is generated by both tearing and folding mechanisms.

Figure 4 shows x-z and x-y projections of the Lorenz attractor generated for control parameter values $(R,\sigma,b)=(278.56,30.0,1.0)$. The first return map can be taken in two ways. If we use two disjoint components for a Poincaré section, as in the case shown in Fig. 2, the return map is as shown in Fig. 5(a). All initial conditions originating on L flow to R, and vice versa. This is a clear signature that one of the two components of the Poincaré section is superfluous. This is the case since the strange attractor can be enclosed in a bounding torus of genus 1. This can clearly be seen in Fig. 4(b). A single component (either L or R) suffices. The first return map on this single component is shown in Fig. 5(b). All extrema are differentiable, clearly indicating that this attractor is generated by folding, not tearing.

As we vary the control parameter values in the Lorenz attractor, we see that there is a transition in the mechanism that generates the strange attractor: from tearing alone (Fig. 2), to tearing and folding (Fig. 3), to folding alone (Fig. 4).

V. IMAGE DYNAMICS

The transformation (1) can be used to map an attractor with rotation symmetry $[R_z(\pi)]$ to an image attractor without symmetry. The Lorenz attractors shown in Figs. 2–4 were mapped to their $2\rightarrow1$ images using this $2\rightarrow1$ local diffeomorphism. The image attractors are shown in Figs. 6(a)–8(a). Each attractor is enclosed in a genus-1 bounding torus, so that the global Poincaré surface of section consists of a single connected component. This component is shown explicitly in each of the Figs. 6(a)–8(a). The first return map of this Poincaré section onto itself is shown in Figs. 6(b)–8(b). These three return maps differ in significant ways.

The return map shown in Fig. 6(b) shows two branches separated by a nondifferentiable extremum. This is a clear signature that tearing occurs in the cover. The dynamical system in Fig. 6(a) is the image of a dynamical system in which tearing is responsible for generating chaotic behavior. The nondifferentiability of the return map at the local maximum is due to the cover singularity which has been mapped into the flow of the image.

The return map shown in Fig. 7(b) shows three branches. The three are separated by a nondifferentiable maximum and

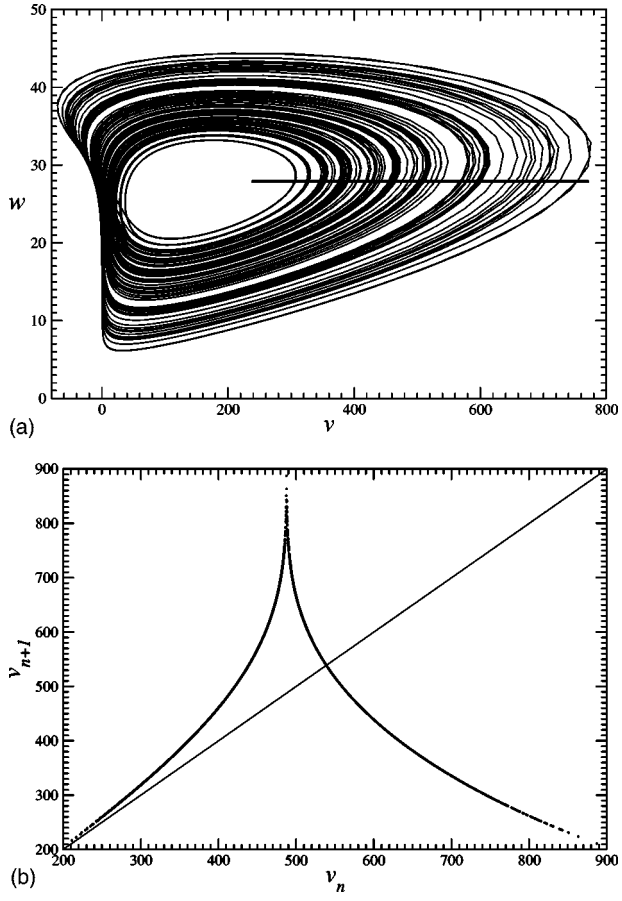

FIG. 6. (a) Projection of the $2\mapsto 1$ image of the Lorenz attractor onto the v-w plane. The global Poincaré section has only the one component shown. First-return map on the Poincaré section shows the branched manifold has two branches. The return map is not differentiable everywhere, showing this is the image of a strange attractor where tearing occurs. Parameter values: $(R,\sigma,b)=(28.0,10.0,8/3)$.

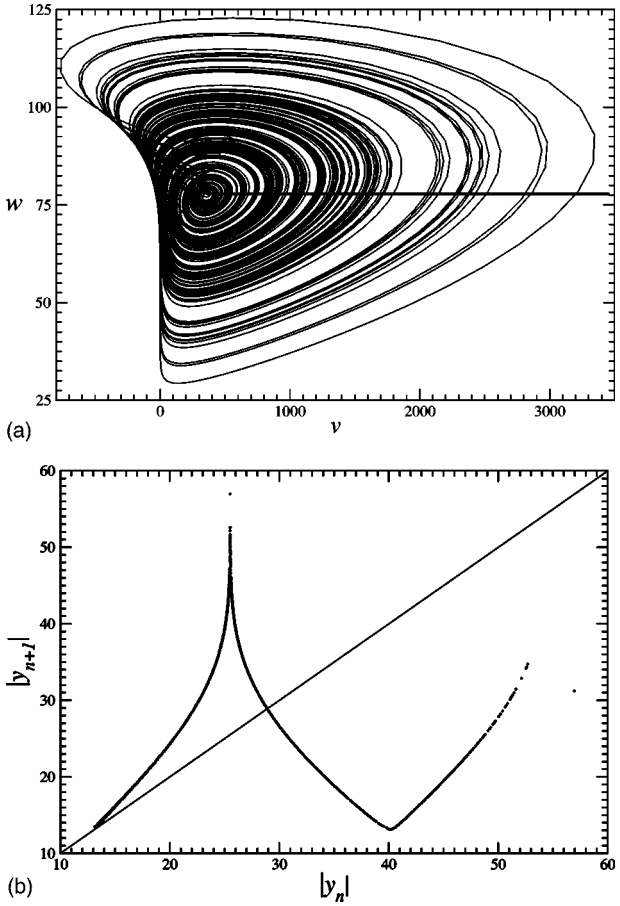

FIG. 7. (a) Projection of the $2\mapsto 1$ image of the Lorenz attractor onto the v-w plane. The global Poincaré section has only the one component shown. First-return map on the Poincaré section shows the branched manifold has three branches. The return map is not differentiable everywhere, showing this is the image of a strange attractor where tearing occurs. The differentiable minimum shows that folding also occurs in the covering attractor. Parameter values: $(R,\sigma,b)=(65.584,13,2.4167)$.

a differentiable minimum. The maximum shows that tearing occurs in the cover, while the differentiable minimum shows that folding also occurs in the cover.

Finally, the return map shown in Fig. 8(b) shows two branches separated by a differentiable minimum. This attractor is generated by folding alone. It is not possible, in this case, to claim that this is the image of a covering attractor, since there is no evidence of tearing in this return map.

Bifurcation diagrams are simple to compute for simple systems and more complicated to compute for more complex systems (genus >1). We compute the bifurcation diagram for the Lorenz attractor as the control parameters are changed according to

$$R = R_0 + \rho(R_1 - R_0),$$

$$\sigma = \sigma_0 + \rho(\sigma_1 - \sigma_0),$$

$$b = b_0 + \rho(b_1 - b_0), \tag{4}$$

where ρ is varied between 0 and 1.3. The parameter triples are $(R,\sigma,b)_0=(28.0,10.0,8/3)$ and $(R,\sigma,b)_1=(278.56,30.0,1.0)$. The results are simply presented by displaying the bifurcation diagram for the $2\rightarrow 1$ images of these equivariant systems. This is shown in Fig. 9. This diagram indicates three distinct regimes of behavior. Tearing occurs for $\rho<1$ and folding occurs for $0.15<\rho$. Both occur in the common range $0.15<\rho<1$. The image branched manifold exhibits two, three, and two branches in these three regions, respectively. The covers have twice as many branches.

The image of a symmetric attractor can sometimes be created without explicitly constructing a local diffeomorphism. This occurs when a strange attractor is constructed by embedding a nongeneric observable of the symmetric attractor. As a particular example, when the z variable of the Lorenz system is used to construct a strange attractor using any kind of embedding, the resulting strange attractor is enclosed in a genus-1 bounding torus and shows folding. However, its return map is similar to that shown in Fig. 6(b), clearly indicating that the fundamental mechanism generating chaos is tearing.

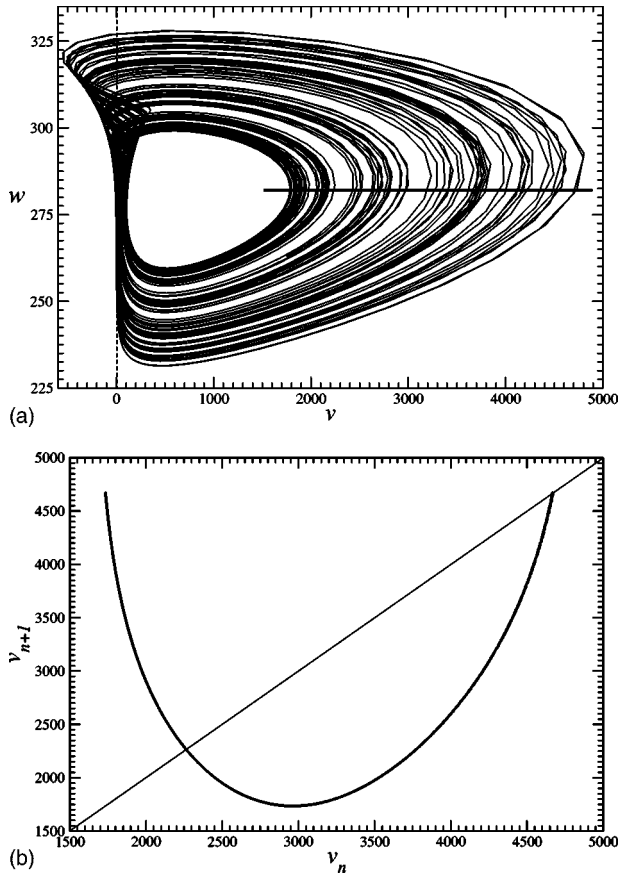

FIG. 8. (a) Projection of the $2\mapsto 1$ image of the Lorenz attractor onto the v-w plane. The global Poincaré section has only the one component shown. First-return map on the Poincaré section shows the branched manifold has two branches. The return map is differentiable everywhere, showing this is a strange attractor where folding occurs. Parameter values: $(R,\sigma,b)=(278.56,30.0,1.0)$.

VI. COVER DYNAMICS

Just as covering attractors can be projected to their images using Eqs. (1) (or an analog for other symmetry), image attractors can be lifted to covers using the inverse mapping. For example, using Eqs. (1) backwards, the Rössler attractor can be lifted to a double cover. In fact, it can be lifted to many topologically inequivalent double covers [8]. A sequence of three double covers of the Rössler attractor is shown in Figs. 10(a)—12(a). These covers are all invariant under rotations $R_z(\pi)$ about the z axis. They differ from each other in the location of the rotation axis.

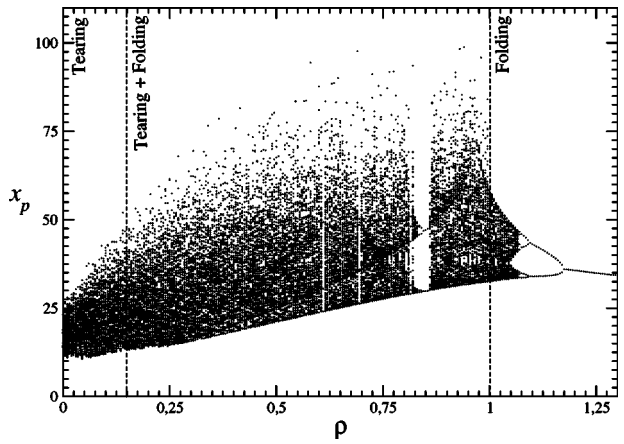

FIG. 9. Bifurcation diagram for the image of the Lorenz attractor, with $|x|$ plotted as a function of ρ.

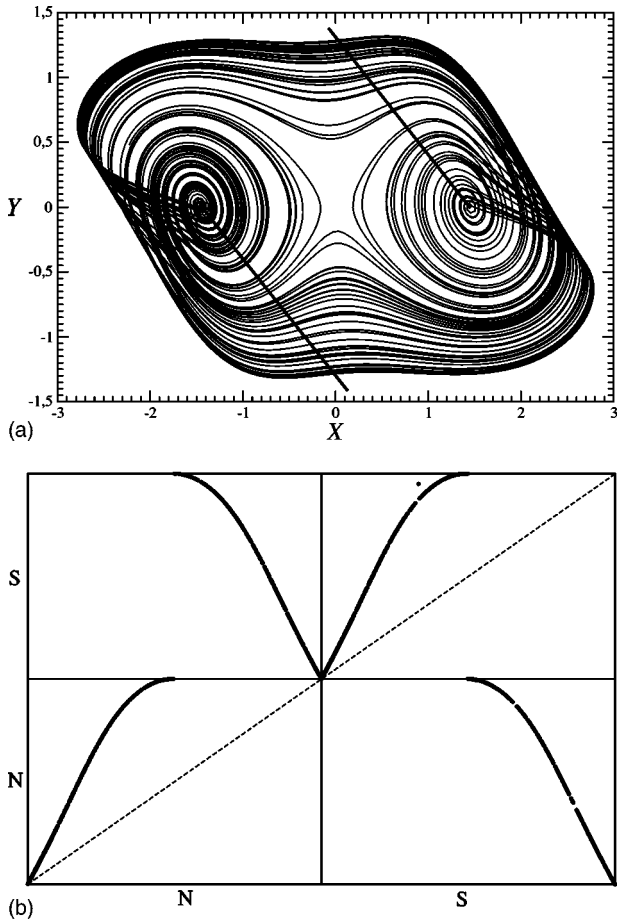

FIG. 10. (a) This double cover of the Rösler attractor can be enclosed in a genus-3 bounding torus. The Poincaré section has two components. (b) First-return map on the Poincaré section has four panels. The discontinuity in the return map shows that this strange attractor is generated by stretching and tearing. The equality of the slopes at the discontinuity shows that it is the symmetric lift of a strange attractor generated in a bounding torus of genus 1 and that the two components of the Poincaré section are related by this symmetry. This strange attractor is described by a branched manifold with four branches. Parameter values: $(a,b,c)=(0.432,2.0,4.0)$.

The cover shown in Fig. 10(a) is created from the Rössler attractor by inserting the rotation axis in the flow. Specifically, it is inserted in the "gap" between branches 0 and 1 in the Rössler attractor. With this nongeneric position of the z axis, the return map shown in Fig. 10(b) exhibits a jump at the point of horizontal tangency. The $R_z(\pi)$ equivariant double cover shown in Fig. 11(a) is constructed by inserting the z axis somewhere in the orientation preserving (0) branch of the Rössler attractor. In this case the jump from component L to R in the Poincaré section splits branch 0. The one-sided derivatives at the discontinuity are equal. This is the signature that the cover is the lift of a strange attractor.

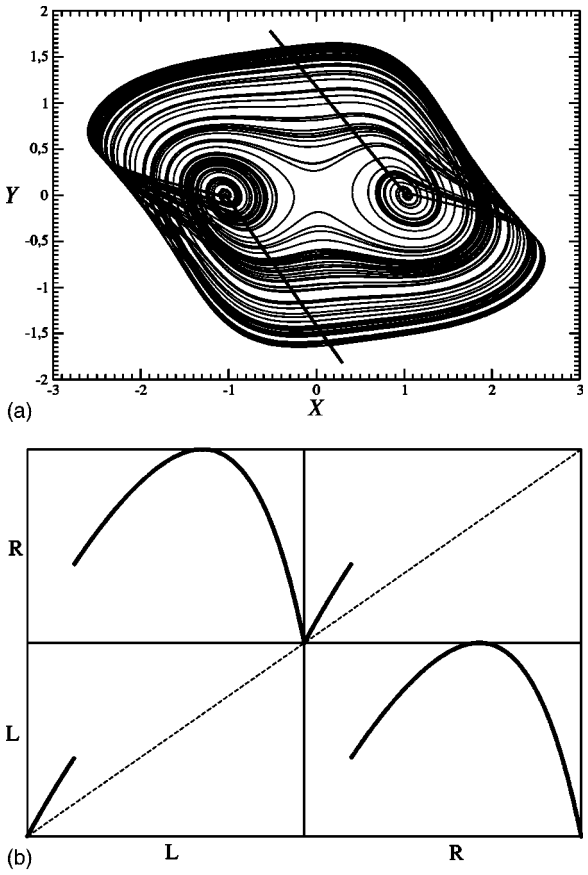

FIG. 11. (a) Another double cover of the Rösler attractor. This can also be enclosed in a genus-3 bounding torus. (b) The discontinuity in the return map shows that this strange attractor is generated by stretching and tearing. The differentiable maxima show that folding also takes place. The equality of the slopes at the discontinuity shows that it is the symmetric lift of a strange attractor generated in a bounding torus of genus 1. This strange attractor is described by a branched manifold with six branches. Parameter values: $(a,b,c)=(0.432,2.0,4.0)$.

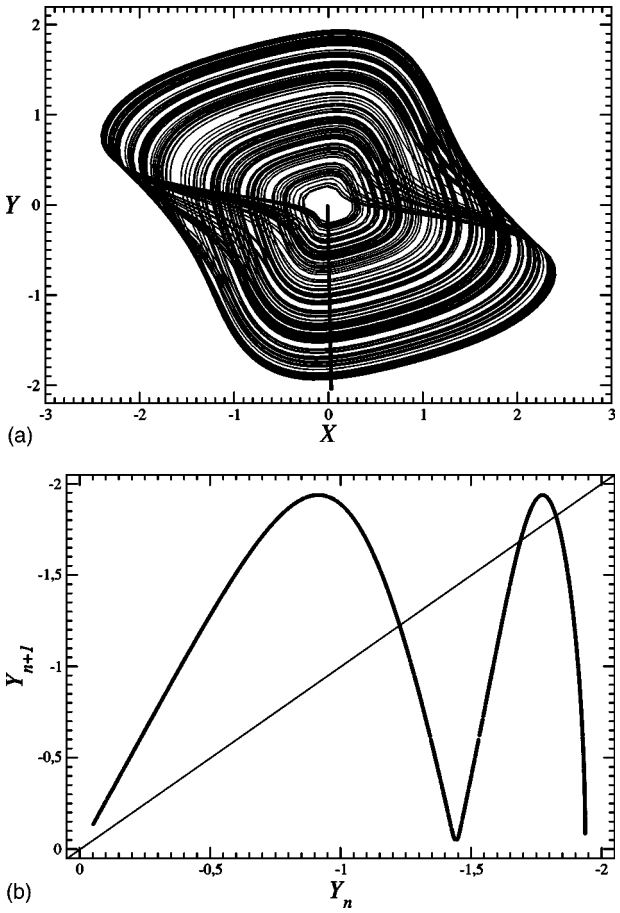

FIG. 12. (a) One double cover of the Rössler attractor that can be enclosed in a genus-1 bounding torus. The Poincaré section has a single component. (b) First-return map on the Poincaré section. This strange attractor is generated by stretching and folding, and is described by a branched manifold with four branches. Parameter values: $(a,b,c)=(0.432,2.0,4.0)$.

The two one-sided derivatives at the jump shown in the return map of Fig. 10(b) are also equal, both equal to zero in that case. The two covers, shown in Figs. 10(a) and 11(a), are both enclosed by genus-3 bounding tori.

The equality of the one-sided derivatives on either side of the jump discontinuity comes about because of the symmetry of the cover. If the symmetry is broken, the one-sided derivatives are not necessarily equal but the jump discontinuity, which is a signature of tearing, will remain.

The double cover shown in Fig. 12(a) is created by inserting the symmetry axis inside the "hole" in the Rössler attractor. This cover has topological index $(n_0,n_1)=(1,1)$ [8]. It can be enclosed in a genus-1 bounding torus. The global Poincaré section has a single connected component. This is shown in Fig. 12(a). The return map on this component is shown in Fig. 12(b). This shows four branches separated by three quadratic extrema. This strange attractor is created by the stretching and squeezing mechanism. From this return map, it is not possible to infer that this strange attractor is the lift of an image attractor, as no discontinuities are present.

VII. SUMMARY

We have described the fingerprints that can be used to identify the origin of low dimensional strange attractors when they are mapped among themselves by local diffeomorphisms. These fingerprints were explained in terms of examples using the Rössler and the Lorenz attractors and simple symmetry groups, but the results are independent of the particular dynamical system and the symmetry group used to create the local diffeomorphism. It is assumed that the source terms for the dynamical systems are smooth.

We can distinguish between the image of an attractor enclosed in a genus-g bounding torus $(g\geqslant 3)$ and an attractor generated by smooth forcing terms in a genus-1 attractor by the degree of smoothness of the first return map. If the map is not differentiable at some extremum, it is an image.

Covers that can be enclosed in a genus-g bounding torus are described by their return maps on a global Poincaré section. The section has exactly $g-1$ components, usually disjoint [9,10]. Discontinuities show where tearing takes place. Tearing is due to the presence of saddle splitting points. Differentiable maxima show that folding also takes place.

Equality of the two one-sided derivatives at a discontinuity shows that the cover is the symmetric lift of a strange attractor whose return map is differentiable—that is, a strange attractor generated by smooth forcing functions in a genus-1 bounding torus.

ACKNOWLEDGMENTS

We thank T. D. Tsankov and A. Nishtala for useful comments. This work was supported in part by NSF Grant No. PHY9987468.

[1] H. G. Solari, M. A. Natiello, and G. B. Mindlin, *Nonlinear Dynamics: A Two-Way Trip from Physics to Math* (IOP Publishers, London, 1996).
[2] N. B. Tufillaro, T. Abbott, and J. Reilly, *An Experimental Approach to Nonlinear Dynamics and Chaos* (Addison-Wesley, Reading, MA, 1992).
[3] E. Ott, *Chaos in Dynamical Systems* (Cambridge University Press, Cambridge, 1993).
[4] J. Birman and R. F. Williams, Topology **22**, 47 (1983).
[5] J. Birman and R. F. Williams, Contemp. Math. **20**, 1 (1983).
[6] R. Gilmore and M. Lefranc, *The Topology of Chaos* (Wiley, New York, 2002).
[7] R. Miranda and E. Stone, Phys. Lett. A **178**, 105 (1993).
[8] C. Letellier and R. Gilmore, Phys. Rev. E **63**, 016206 (2001).
[9] T. D. Tsankov and R. Gilmore, Phys. Rev. Lett. **91**, 134104 (2003).
[10] T. D. Tsankov and R. Gilmore, Phys. Rev. E **69**, 056206 (2004).
[11] O. E. Rössler, Phys. Lett. **57A**, 397 (1976).
[12] E. N. Lorenz, J. Atmos. Sci. **20**, 130 (1963).